Roadway traffic monitoring from an unmanned aerial vehicle

B. Coifman, M. McCord, R.G. Mishalani, M. Iswalt and Y. Ji

Abstract: Roadway networks span large distances and can be difficult to monitor. Most efforts to collect roadway usage data either require a large fixed infrastructure or are labor intensive. Technological advances in electronics and communication have recently enabled an alternative, unmanned aerial vehicles (UAVs). UAVs capable of carrying sensors and communications hardware to relay data to the ground are becoming available on the commercial market. UAVs can cover large areas and focus resources. They can travel at higher speeds than ground vehicles and are not restricted to travelling on the road network. We investigate the use of a UAV to monitor roadway traffic and develop and demonstrate several applications using data collected from a UAV flying in an urban environment. We describe our use of the data to determine level of service, average annual daily traffic, intersection operations, origin–destination flows on a small network, and parking lot utilization. Our ability to determine these measures illustrates the feasibility of extracting useful information from images sampled from a UAV for both off-line planning and real-time management applications, and our discussion of the methods indicates the challenges and opportunities images obtained from such a platform pose and entail.

1 Introduction

Roadway networks span large distances and can be difficult to monitor. Most efforts to collect roadway usage data either require a large fixed infrastructure or are labor intensive. Conventional traffic surveillance relies on a set of detectors (including cameras) deployed at fixed locations, requiring a high density of detectors to monitor changing conditions throughout the network. When information is needed from beyond the range of these fixed detectors, personnel are usually deployed to assess conditions. Technological advances in electronics and communication have recently enabled an alternative to an inflexible fixed network of sensors or the labor-intensive and potentially slow deployment of personnel. Unmanned aerial vehicles (UAVs) capable of carrying a video camera, geo-positioning sensors and communications hardware to relay data to the ground are becoming available on the commercial market. Examples include the MLB-BAT [1] and GeoData Systems-Airborne Data Acquisition System [2]. Many of these low cost aircraft are capable of sophisticated autonomous flight.

IEE Proceedings online no. 20055014

doi:10.1049/ip-its: 20055014

Paper received 12th December 2005

B. Coifman, M. McCord, R. G. Mishalani, M. Iswalt and Y. Ji are with the Department of Civil and Environmental Engineering and Geodetic Science, The Ohio State University, Columbus, OH, 43210. USA

B. Coifman is also with the Department of Electrical and Computer Engineering, The Ohio State University, Columbus, OH, 43210, USA

M. McCord and M. Iswalt are also with the Knowlton School of Architecture, City and Regional Planning, The Ohio State University, Columbus, OH, 43210, USA

E-mail: coifman.1@osu.edu

In this paper we investigate the feasibility of using a UAV to monitor traffic and develop several applications. As noted in [3], UAVs can cover a large area and focus resources. They can travel at higher speeds than ground vehicles and UAVs are not restricted to travelling on the road network. With autonomous flight capabilities UAVs can potentially free personnel from time-consuming travel to remote field locations.

To explore the benefits of UAVs in this context, on 22 July 2003 a set of experiments was conducted on the campus of The Ohio State University in Columbus using the BAT III technology [1] carrying a payload of two video cameras. The UAV flew at an altitude of 150 m and an air speed around 50 km/h while transmitting video images to the ground station in real-time. The flight lasted almost 2 h and data were collected from several facilities. Fig. 1*a* shows a map of the study area, roughly 2 km east-west and 2.2 km north-south (adapted from [4]). This urban setting included many intersections and parking lots as well as a freeway, SR 315, running north/south through the middle of the map. As described below, five applications were examined: measuring level of service (LOS), estimating average annual daily travel (AADT), examining intersection operation, measuring origin–destination (OD) flows on a small network, and measuring parking lot utilisation. Fig. 1*b* shows a schematic of the primary roadways from Fig. 1*a* used in this study.

The subsequent descriptions are intended to provide the main concepts and methods applied to derive useful information for both off-line planning and real-time management applications. Moreover, the extracted information is presented in some detail. The purpose is to demonstrate the feasibility of extracting useful information from images sampled from an UAV and illustrate the challenges and opportunities such images pose and entail.

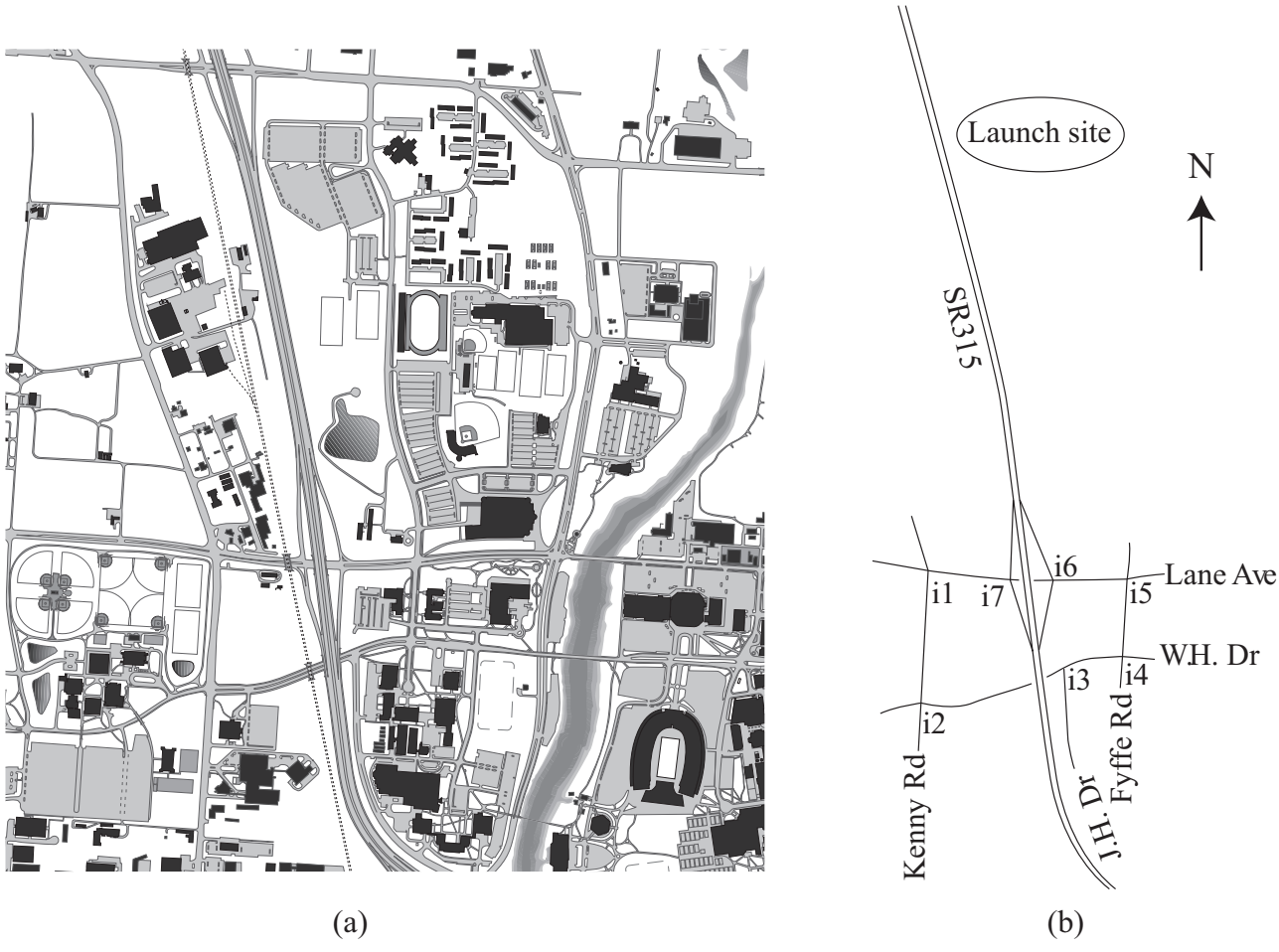

Fig. 1

a Map of the study area, roughly 2 km across
b Schematic of the primary network from the map (at the same scale) used in this study

2 LOS measurement and AADT estimation

The UAV made one round trip along the southern 1.5 km of SR 315 shown in Fig. 1. The video images from this trip were used to investigate LOS and AADT, respectively reflecting instantaneous and long-term traffic conditions. Density (vehicles/km) was used to measure LOS, while flow (vehicles/h) was used to estimate AADT. As discussed below, two different methods of estimating freeway density and flow were developed. The first method uses still frames, and the second method exploits information from a series of frames using Edie's generalised definitions over time and space [5].

2.1 Method 1: density and flow from still frames

The numbers of passenger cars and trucks can be obtained directly from still video images. Given these numbers and the length of imaged roadway segment they occupy, the traffic density is commonly defined as:

$$k = \frac{\mathrm{PC} + \mathrm{TR} \cdot 1.5}{L} \tag{1}$$

where,

L = the segment length in km;
PC = the number of passenger cars in the imaged portion of the segment;
TR = the number of trucks in the imaged portion of the segment.

Here the most difficult aspect is measuring L along the roadway accurately. For this study we used a geo-referenced aerial photo and a geographic information system (GIS) to measure distance between observed landmarks. Conceivably the camera could be calibrated so that distance along the ground could be extracted from the UAV views and distance travelled by the UAV. In any event, given the density calculated in (1), the hourly volume can be estimated from the fundamental equation,

$$q^H = k \cdot \bar{v} \tag{2}$$

where,

$\bar{v}$ = space mean speed.

Although one cannot measure speed from a single still frame, it can either be estimated from the posted speed limit or from the video stream. In this study two different approaches were used to estimate speed. The first speed estimate used the GIS to measure the distance between two points visible in the given still frame. The video stream was then used to measure travel times across this segment for as many vehicles as possible. The space mean speed was then estimated by the arithmetic mean of the measured speeds across the link, i.e.

$$\bar{v} = \frac{1}{m}\sum_{i=1}^{m}\frac{L}{t_i} \tag{3}$$

where,

t_i = travel time of the i-th vehicle in the segment of length L,
m = the total number of vehicles measured.

The second speed estimate is intended to be used when it is difficult or impossible to match the start and end of a

segment with landmarks in the GIS. In this case we selected several vehicles at random from the given still frame. Each vehicle was tracked over several seconds, we counted the number of lane markers passed and recorded the travel time. Once more the space mean speed was estimated by the arithmetic mean of the measured speeds, i.e.

$$\bar{v} = \frac{1}{m}\sum_{i=1}^{m}\frac{n_i \cdot l}{t_i} \tag{4}$$

where,

n_i = the number of lane markers that the i-th vehicle passed,

l = the distance from the beginning of one lane marker to the beginning of the next, (12.2 m was taken from the design specifications and used here),

t_i = travel time of the i-th vehicle.

This method was applied to many frames, including the five shown in Fig. 2.

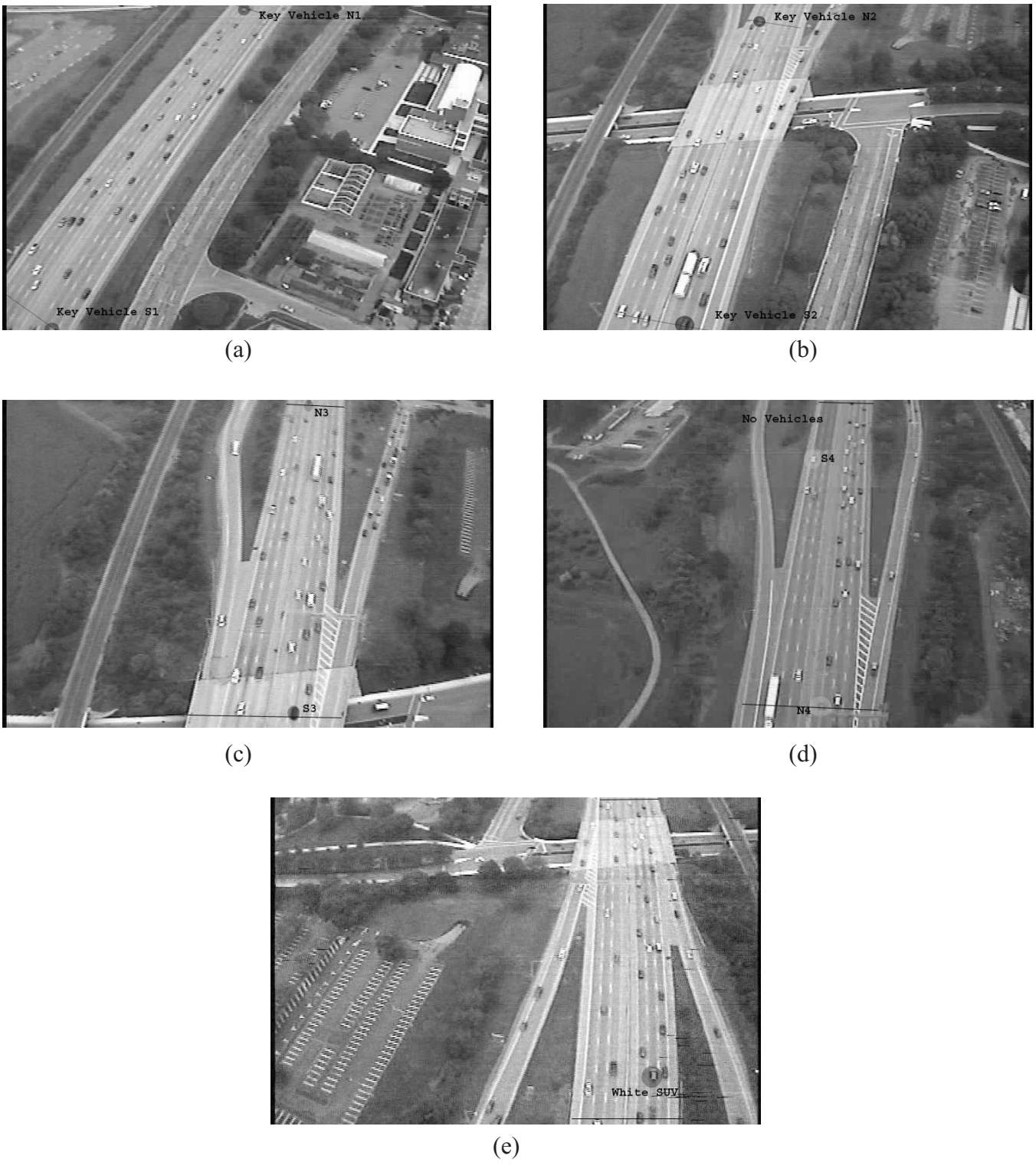

Fig. 2 *Five sample frames used to estimate flow, density, LOS and AADT*
a–f Correspond respectively to frames 1–5

2.2 Method 2: density and flow from a series of frames

At any given instant the UAV sensor only views a small portion of the roadway. Normal fluctuations in the traffic could cause large variations in density measured from a still frame. The use of individual still frames to estimate density discards a wealth of information in the video stream. As the UAV flies over the traffic the sensor observes conditions over a longer time and distance, but the field of view (FOV) continually changes, making difficult the task of measuring conventional density or flow. Edie's generalised definitions [5] over time and space can accommodate this changing FOV. For an arbitrary region, A, of the time–space plane the flow, density and space mean speed are defined, respectively, as,

$$q(A) = \frac{d(A)}{|A|} \tag{5a}$$

$$k(A) = \frac{t(A)}{|A|} \tag{5b}$$

$$\bar{v}(A) = \frac{d(A)}{t(A)} \tag{5c}$$

where,

$d(A)$ = the total distance travelled by all vehicles in region A,

$t(A)$ = the total time spent by all vehicles in region A,

$|A|$ = the 'area' covered by region A in the time–space plane.

Using the video from the northbound flight over SR 315, vehicle trajectories were constructed for the southbound traffic, sampled at 2 s intervals using positions calculated from the GIS. This procedure was repeated in each lane. In a similar fashion the FOV of the southbound lanes was extracted from the video. Fig. 3 shows in the time–space plane the resulting trajectories from the inside lane with solid lines and the FOV with a shaded region for 20 s. In the event that a vehicle leaves the FOV before the next observation, the trajectory is extended linearly to the FOV, as shown with dashed lines at the ends of most trajectories. The flow and density over the region spanned by the FOV were obtained from the vehicle trajectories by applying (5*a*) and (5*b*).

In fact one does not need the vehicle trajectories, only the times and locations where vehicles enter and leave the FOV. Since time and distance are summed across all vehicles it is only important to differentiate between entering and leaving the region, without tracking the vehicles through the FOV, i.e.

$$\begin{aligned} d(\text{FOV}) &= \sum_i \left(x_{\text{exit}}(i) - x_{\text{enter}}(i)\right) \\ &= \sum_i x_{\text{exit}}(i) - \sum_i x_{\text{enter}}(i) \end{aligned} \tag{6a}$$

$$\begin{aligned} t(\text{FOV}) &= \sum_i \left(t_{\text{exit}}(i) - t_{\text{enter}}(i)\right) \\ &= \sum_i t_{\text{exit}}(i) - \sum_i t_{\text{enter}}(i) \end{aligned} \tag{6b}$$

where the i-th vehicle enters the FOV at $(x_{\text{enter}}(i), t_{\text{enter}}(i))$ and exits at $(x_{\text{exit}}(i), t_{\text{exit}}(i))$. The boundaries of the FOV need to be specified as accurately as possible to measure |FOV| precisely. Equations (6*a*) and (6*b*) can be summed across individual lanes, or the entire roadway can be processed without regard to which lane a vehicle is travelling in.

2.3 LOS and AADT

Using the average density across all lanes from either method ((1) or (5*b*)), the LOS can be determined directly from the 'Highway Capacity Manual' tables, as reproduced in Table 1 (adapted from [6]). The measured density for the southbound traffic in the five frames

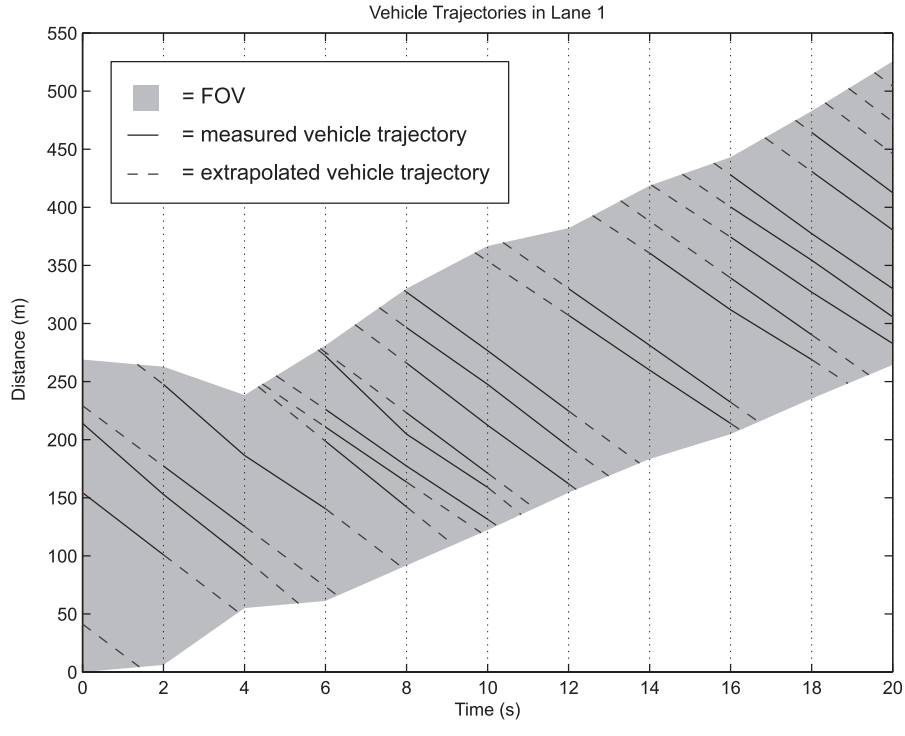

Fig. 3 *Example of extracted vehicle trajectories and the UAV FOV on 315-South*

from Fig. 2 and the video series mentioned above and the resulting LOS measurements are presented in Table 2.

AADT is estimated following the methodology of [7], using either estimate of hourly volume discussed above, in this case, (2) and (3) or (5*a*),

$$\mathrm{AADT} = q^H \cdot F^{8-9} \cdot 24 \cdot F^{\mathrm{Tu,July}} \tag{7}$$

where,

F^{8-9} = time-of-day factor published by the Ohio Department of Transportation (ODOT) for 8–9 am, (the time of day when the video was taken),

$F^{\mathrm{Tu,July}}$ = seasonal factor published by ODOT for a Tuesday in July, (the day and month when the video was taken).

Naturally the estimates from (2) and (7) are somewhat noisy. Table 2 shows the estimated q^H from each of the five frames for the southbound traffic with a range between largest and smallest value spanning 4000 veh/h and resulting AADT range spanning 60 000 veh/day. For comparison sake the official ODOT AADT for the link measured with conventional terrestrial methods is also presented in the table.

The still frame method is easy to apply; however, using individual frames to estimate density and flow is problematic because each frame represents a very small sample size. The relatively short roadway sections used in each density and flow calculation in the still frame method can amplify even the smallest traffic fluctuation, rounding errors arising from the integer nature of vehicle counts and detection errors. These errors are further amplified when scaled up to daily totals and are a major factor in the variability between AADT frame estimates.

As was shown in [8], even such noisy estimates can be valuable when they are combined appropriately with other noisy estimates based on older ground-based data. In addition, the impact of this noise can be reduced by integrating information across several independent observations. Taking the average across the five frames using Method 1, and then separately calculating the generalised flow from the video stream using Method 2, notice from Table 2 that both averages are close to one another and within 16 percent of the ODOT AADT. The improved accuracy is probably due to the fact that two averages incorporate more vehicles over a larger region of the time–space plane compared to the still frame method applied to a single frame.

Table 1: Level of service classification density range (veh/km/lane)

LOS	Basic freeway segments
A	0–7
B	7–1
C	11–16
D	16–22
E	22–28
F	over 28

3 Intersection operations

The majority of the flight time was devoted to monitoring intersections. First the UAV circled the small network shown in Fig. 1*b*, counter clockwise past i1-i2-i4-i5, then reversed direction, flying clockwise past i1-i5-i4-i2. Fig. 4*a–c* shows an example of the views from the UAV while circling counter clockwise. Then the UAV circled individual intersections for several minutes, first i1, then i4, i5, and the diamond interchange of i6 and i7. Fig. 4*c, d* shows opposing views of i1 and illustrates how the view changed while circling i1.

These video segments were used to analyse intersection operations. Most of the analysis was based on common queuing measures. Two methods of measuring intersection queue lengths were examined. The first method used input–output flows to measure point queues on intersection approaches. To facilitate measuring the point queues, a straightforward computer program was written and used to track the times when vehicles pass two points on each approach. These data allowed for the construction of vehicle arrival and departure curves. Queues, signal timings, arrival rates, and turning movements were all derived from these curves. The second method examined spatial queues and consisted of sampling spatial queue lengths on intersection approaches at fixed time intervals.

3.1 Point queues

Using the computer interface to record vehicle arrivals and departures on each approach at each intersection that was circled, the cumulative arrival and the cumulative departure curves were obtained. On a given approach the arrival curve, $A(t)$, was measured at a point far enough upstream of the intersection that queues rarely overran the location while being close enough to the intersection that the point was usually within the FOV. In the rare event that either of these assumptions was violated, the analysis was suspended until the violated assumption was restored. The departure curve, $D(t)$, was measured at the stop bar and vehicle turning movements were recorded through different key presses using the computer interface as the vehicles passed. Following normal queuing theory the arrival curve was shifted forward in time by a constant, free flow travel time to yield the virtual arrival

Table 2: Density, Flow, AADT and LOS Results of SR 315 Southbound

	Frame	Video Segment	Density (Veh/km/lane)	LOS	q^H (Veh/hour)	AADT (Veh/day)
Method 1	1	315N	25.5	E	9857	146 214
Method 1	2	315N	26.6	E	10286	152 571
Method 1	3	315N	20.7	D	6000	89 000
Method 1	4	315S	35.9	F	10400	154 267
Method 1	5	315S	31.7	F	9200	136 467
Method 1: average			28.1	F	9149	135 704
Method 2		315N	29.8	F	8399	124 581
ODOT AADT						117 180

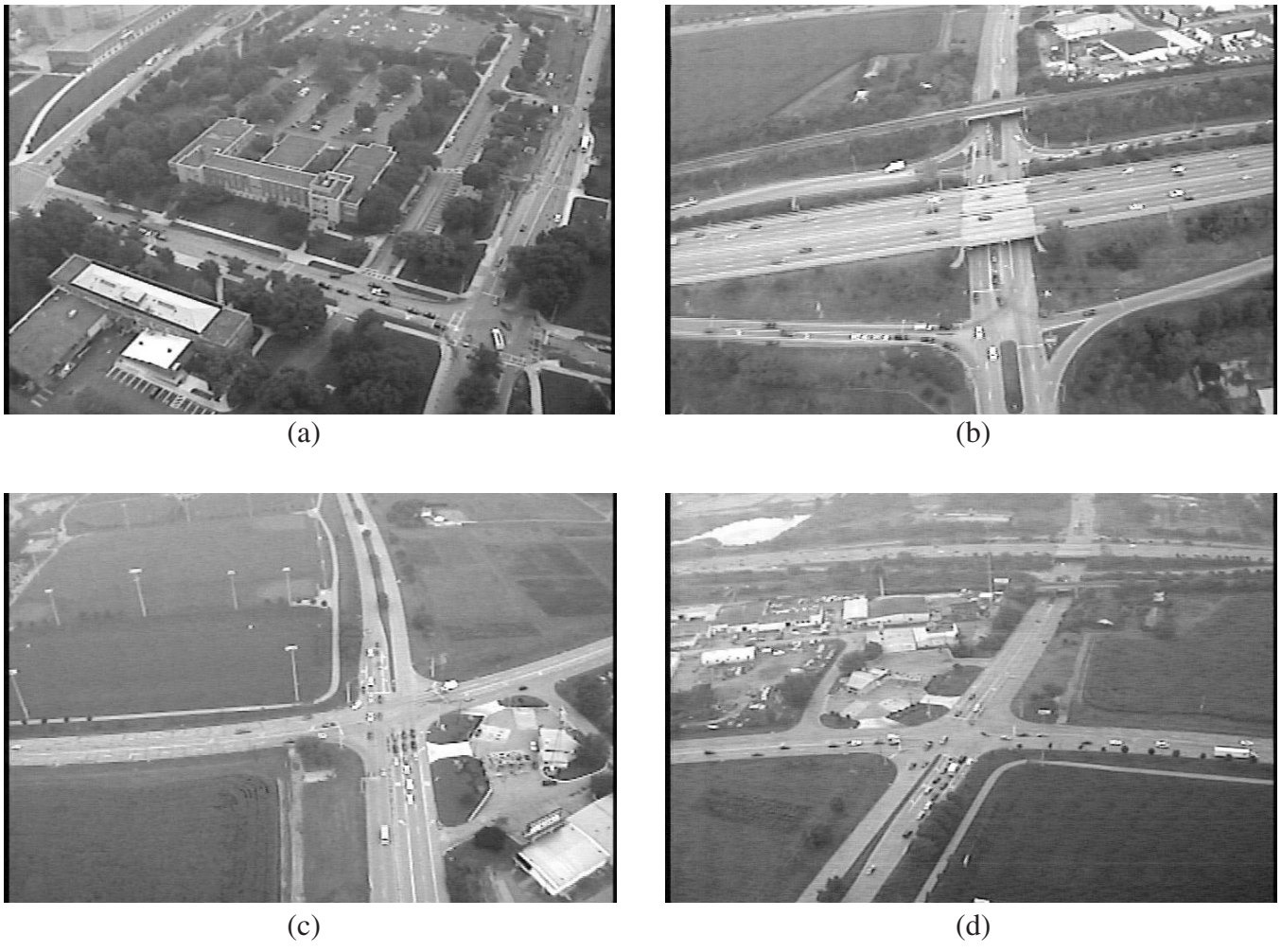

Fig. 4 Sample images while circling the network and individual intersections
a Viewing east with i5 on the far left and i4 on the right
b Viewing west i6 then i7
c Viewing west i1
d Viewing east i1

curve at the stop bar, $V(t)$. The time shift was estimated empirically on each approach by measuring several vehicles traversing the distance between the two locations under free flow conditions. In this way, $V(t)$ reflects the time vehicles would have passed the stop bar if there were no delay between the two points. The point queue at any instant, then, is simply,

$$Q(t) = V(t) - D(t) \tag{8}$$

Fig. 5 shows two cycles from the point queue model of the eastbound approach to i1. The other approaches were similarly processed. Fig. 5*a* shows $A(t)$, $V(t)$ and $D(t)$. On this approach the free flow travel time was determined to be 6 s. The traffic signal indications were not visible at the resolution of the UAV video. The signal phasings in Fig. 5*b* were extracted by watching vehicle movements on all four approaches. The validity of these extracted phasings was verified at this intersection using concurrent video filmed on the ground. There are two periods where $D(t)$ is nearly horizontal, corresponding to the red phase. The small number of departures observed during these periods come from vehicles turning right on red. Fig. 5*c* shows $Q(t)$ using (8). Queue growth after the signal turns red and the subsequent decay after the signal turns green are clearly evident. The observed peaks correspond to queue lengths just before $D(t)$ exhibits saturation flow at the start of the green phase.

3.2 Spatial queues

The point queue accurately captures delay, but assumes that all the delay occurs at the stop bar. In fact most of the delay is takes place upstream of the stop bar. As the queue grows upstream of the stop bar, vehicles enter the queue sooner than would be predicted by a point queue model, consuming some of the free flow travel time while in the queue. Such spatial queuing models capture greater detail of what is experienced by travellers but lead to complications when trying to extract delay and other metrics. Recognising the spatial nature of real queues is important, since a queue can impede the operation of the network if it overruns an upstream intersection (a good overview of the trade offs between point and spatial queue models can be found in [9]).

Therefore, in the second method, spatial queues at intersections were measured at regular time intervals by counting the number of vehicles queued at an instant in time. Sampling spatial queues in this fashion precludes delay measurement but accurately captures the spatial extent of the queue and can be done very quickly. Since each measurement only needs to capture an instant, this method utilised the video from circling the network in

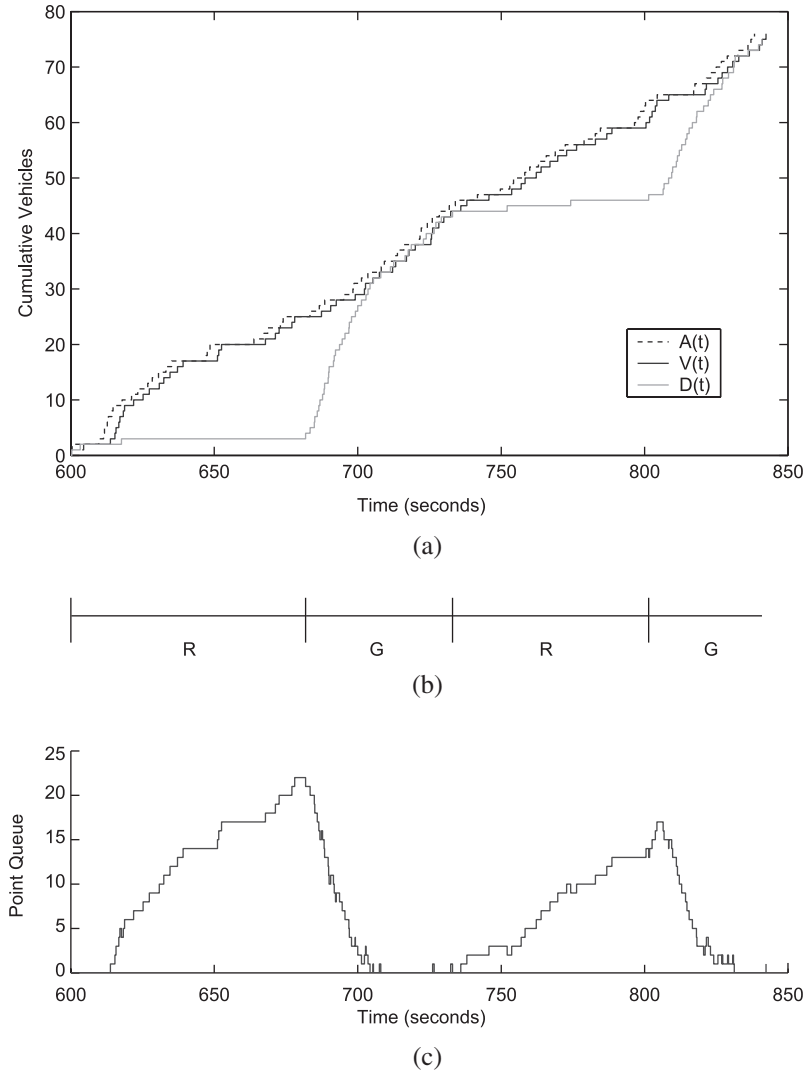

Fig. 5

a Cumulative arrivals and virtual arrivals at the stop bar for two cycles from the eastbound approach to i1
b The signal phasing on this approach
c The measured point queue lengths

addition to the video from circling individual intersections. An observer manually counted the number of vehicles in the queue by lane at fixed intervals for each approach to i1, i5, i6, and i7. A 10 s sapling interval was used while the UAV circled a particular intersection. A given intersection was only in view for 10–30 s when the UAV circled the network, and a 5 s sampling interval was used to provide more observations to be used in the comparisons.

Fig. 6 presents the average spatial queue length for i1 obtained from this method. This figure compares average spatial queue lengths obtained during intervals when the UAV circled a particular intersection to those obtained during periods when the UAV circled the larger network. If the intermittent observations obtained while circling the network all fall in the same phase of the cycle, the queue measurements would show disproportionately longer average queues on the approaches that were imaged during red phases and disproportionately shorter average queues on the approaches that were imaged during green phases. Provided care is taken to ensure that the observations while circling the network do not fall at the same point in the cycle, it should be possible to use a UAV to monitor concurrently the queue lengths at many intersections, e.g. the seven intersections in the small network of Fig. 1*b*. Since the empirical results in Fig. 6 come from different times of the day (roughly an hour apart), at this time it is not possible to conclusively confirm or refute the hypothesis that intermittent sampling while circling a large network is sufficient. However, the results do fall within expectations. Between the two data sets, three of the four approaches had average queue lengths within two vehicles. The fourth approach had much longer queues when the UAV circled the network, which occurred during the morning peak period, and much shorter queues when the UAV circled the intersection, which occurred after the peak.

4 Origin–destination estimation

We used the UAV video while circling intersections i6 and i7 in conjunction with video taken from ground-based cameras at i1 to determine OD flows on this small network. The network is shown in Fig. 7*a* superimposed on an aerial photo. The origins were defined to be the approaches to the diamond interchange, i6 and i7, and the destinations were the three branches from i1. Fig. 7*b* shows a simplified schematic of the network highlighting

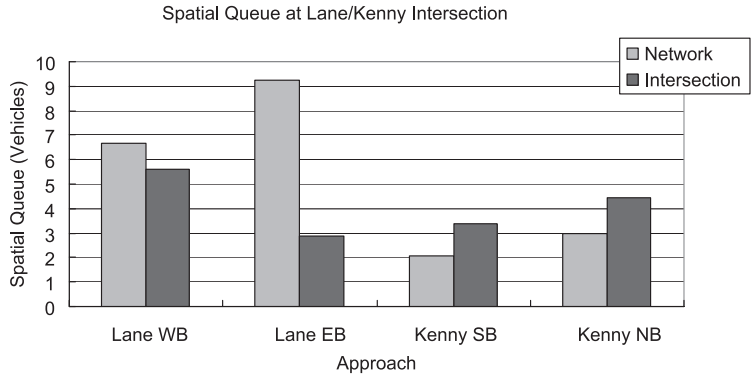

Fig. 6 *Average spatial queue comparison between observations while circling the network and later while circling the intersection*

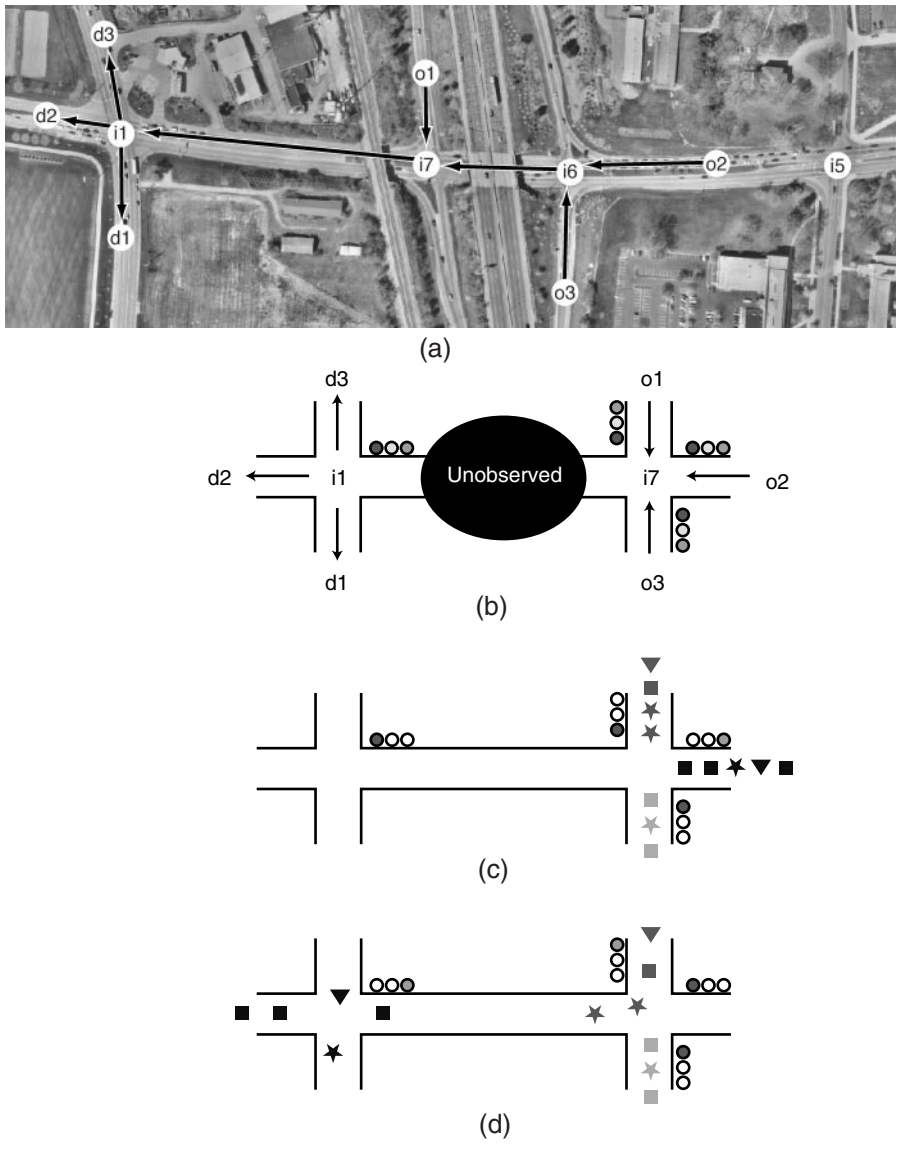

Fig. 7

a The OD network superimposed on an aerial photo
b A simplified schematic of the network, most of the roadway between i7 and i1 went unobserved
c Example where westbound traffic from o2 just received a green light, each origin is given one shade and each destination one symbol
d Continuation of the example a few seconds later as the platoon from o2 passes i1 and a new platoon starts from o1

the fact that most of the roadway between i7 and i1 went unobserved. The primary goal of this effort is to match observations across this unobserved region and measure network OD flows. To this end a methodology was developed in which we match platoons of vehicles from the various origins to an approach feeding into the downstream intersection, and subsequently the vehicles are followed through to their respective destinations. The platoon-matching method avoids the need to match individual vehicles, since any unobserved reordering

within a platoon from a given origin will not change the proportion of vehicles bound for a given destination.

The computer interface developed to study intersection operations was used here to record the origins, departure times and lanes in which vehicles depart the upstream intersection FOV. Similarly, the process was repeated for the vehicles at the downstream intersection, from arrival in the downstream FOV to their final destination. Within each intersection the vehicle movements were followed, yielding a map to the particular origin or destination. A few vehicles departed the network at the freeway on-ramps, which were visible from the UAV view. These vehicles were excluded from further analysis.

The number of vehicles at the upstream and downstream intersections, along with their origins and destinations, represent the marginal totals of the OD flows, i.e. the number of vehicles that originate at an origin or terminate at a destination. Table 3 shows the origin and destination totals. In principle the measurement of flows between origins and destinations could theoretically be accomplished through exact one-to-one

Table 3: Origin and destination totals

	Description	Number of vehicles
O1	315S	51
O2	315N	55
O3	Lane WB	16
Total O's		122
D1	Kenny SB	34
D2	Lane WB	82
D3	Kenny NB	6
Total D's		122

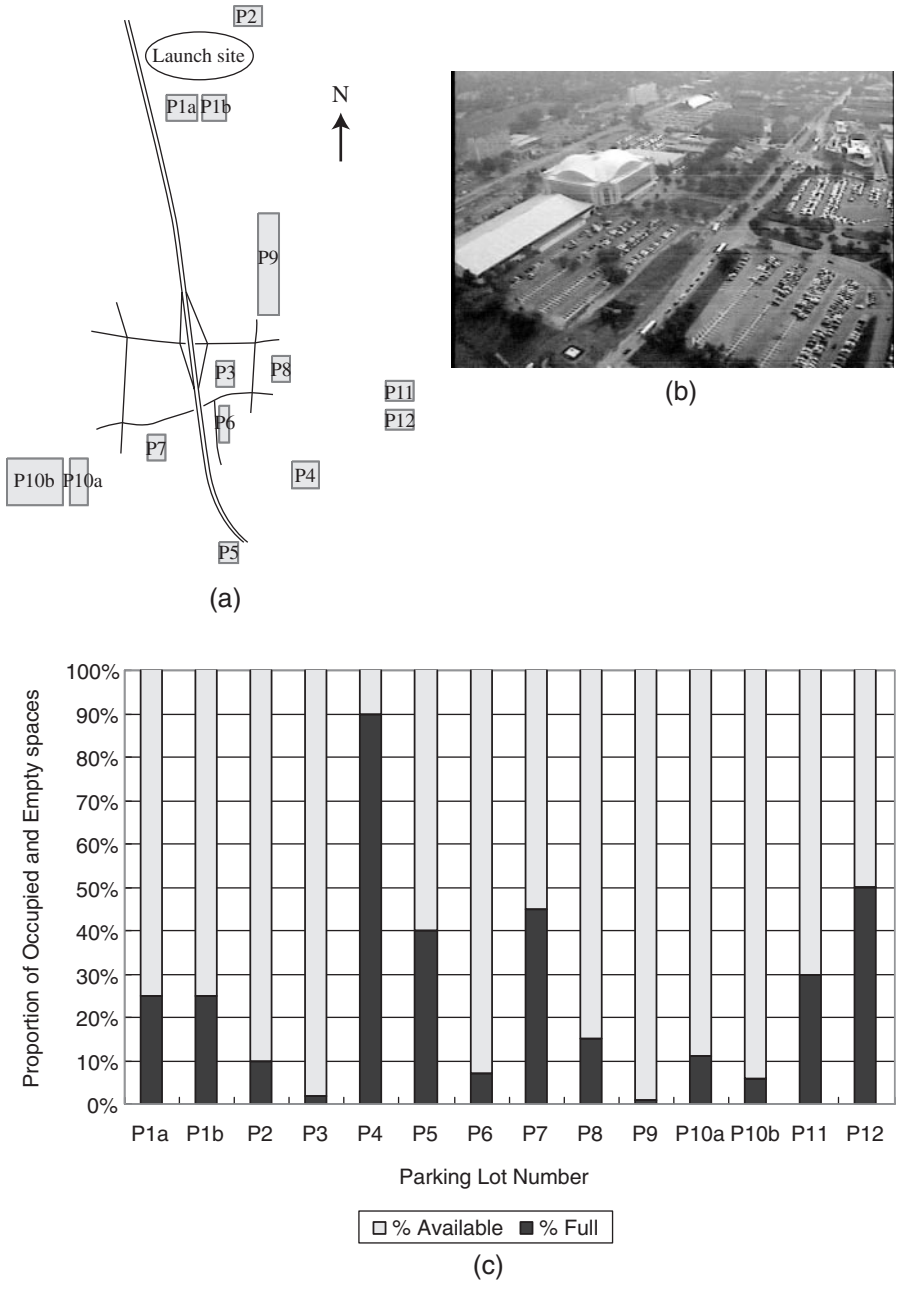

Fig. 8

a Schematic showing the location of observed parking lots relative to the primary network
b A sample view from the flight showing P11 to the left and P12 to the right in the foreground
c Measured parking lot utilization

Table 4: Complete OD matrix

	D1	D2	D3	Sum O
O1	18	32	1	51
O2	11	42	2	55
O3	5	8	3	16
Sum D	34	82	6	122

matching of all vehicles between origins and destinations. However, this task would prove tedious over large samples, and in this case would be very difficult, if not impossible, given the resolution of the imagery and the non-overlapping fields of view obtained in the upstream UAV video and the downstream ground camera views. Instead, we matched distinct vehicle platoons between the intersections.

Key to the feasibility of this methodology is the fact that the headway between platoons is normally much larger than the headway between vehicles within platoons. As the upstream signal cycles through approaches, the clearance intervals introduce these larger headways between platoons from the various origins. Large headways mean overtaking between platoons is generally uncommon, and if it does occur, it will only be among the vehicles at the end of the platoon. Moreover, reordering of vehicles within platoons due to overtaking will not impact OD flows, thus allowing the use of the simple first-in-first-out assumption. Fig. 7*c, d* illustrate the process, where each origin is given one shade and each destination one symbol. In this hypothetical example there is a gap after the platoon from o2 has departed the upstream intersection (on the right) before the platoon from o1 is released.

Table 4 shows the resulting OD flows from the platoon-matching procedure applied to the empirical data. In the platoon matching method, measurement errors are inevitable during data reduction. Such errors could change the derived OD flows. The impact of such errors are investigated in [10], where it is shown that many of these errors can be detected using the observed data.

5 Parking lot utilisation

The last few minutes of the UAV flight were devoted to flying over several large parking lots shown in Fig. 8*a*, namely P10a, P10b, P11, P12, P9, P1a, and P1b (in that order). Fig. 8*b* shows P11 to the left and P12 to the right in the foreground with a third lot behind them on the right. Throughout the flight many other parking lots were visible. These comprise the remaining labelled lots in Fig. 8*a* (Figs 8*a* and 1 are to the same scale). In fact, P3 and P8 are visible, respectively, in the bottom and top of Fig. 4*a*. The capacity of the parking lot, the number of available parking spaces, and the number of occupied parking spaces can be acquired from the video. Such information would be useful for directing commuters or event traffic to the best lots and in providing planning data on parking needs. Compared to ground-based crews, a UAV can quickly fly among multiple parking lots to provide many more repeated samples of the usage in a given time. Fig. 8*c* shows the utilisation of the parking lots. Lot 4 is nearly full, while most of the remaining lots were relatively empty, since this was summer quarter.

6 Conclusions

This paper presented methodological developments to exploit UAV data for multiple applications. The applications discussed here were LOS, annual average daily traffic, intersection operations, OD flows on a small network and parking lot utilisation. All these applications were demonstrated from less than 2 h of flight time. Most of the data reduction in this study was done manually using computers to simplify many of the tasks. If UAVs were used on a large scale for any of these applications, it is likely that additional aids would be developed to assist this process, e.g. software to keep the FOV on the road or make it easier to measure distances in the FOV, and hardware, such as multiple cameras or specialised lenses, to extend the FOV. In the long term, it is likely that many of the tasks could be automated.

7 Acknowledgments

This study was funded through a grant to the National Consortium for Remote Sensing in Transportation-Flows (NCRST-F) from the US Department of Transportation. The efforts of Steve Morris from MLB in providing the aircraft and operator for the field experiment and of Keith Redmill from OSU in providing logistical support are particularly appreciated. The authors also acknowledge the help of the many agencies—including the Federal Aviation Administration and the Columbus Police Department—and their staff that enabled the UAV experiment.

8 References

1 MLB: 'MLB Company', http://spyplanes.com, accessed December 2005
2 GeoData Systems: 'GeoDataSystems', http://www.geodatasystems.com, accessed December 2005
3 Coifman, B., McCord, M., Mishalani, R., and Redmill, K.: 'Surface transportation surveillance from unmanned aerial vehicles'. Proc. 83rd Annual Meeting of the Transportation Research Board, Washington, DC, January 2004
4 Ohio State University Department of Physical Facilities: http://www.physfac.ohio-state.edu/mapping, accessed July 2003
5 Edie, L.: 'Discussion of traffic stream measurements and definitions'. Proc. 2nd Int. Symp. Theory of Traffic Flow, 1963, pp. 139–154
6 TRB: 'Highway Capacity Manual' (Transportation Research Board, 2000)
7 McCord, M., Yang, Y., Jiang, Z., Coifman, B., and Goel, P.: 'Estimating AADT from satellite imagery and air photos: empirical results', *Transp. Res. Rec.*, 2003, **1855**, pp 136–142
8 Jiang, Z., McCord, M., and Goel, P.: 'Improved AADT estimation by combining information in image- and ground-based traffic data', *ASCE J. Transp. Eng.*, 2006, in press
9 Erera, A., Lawson, T., and Daganzo, C.: 'Simple, generalized method for analysis of traffic queue upstream of a bottleneck', *Transp. Res. Rec.*, 1998, **1646**, pp. 132–140
10 Mishalani, R., McCord, M., Coifman, B., and Iswalt, M., Ji: 'Platoon based origin destination estimation', Proc. of Applications of Advanced Technology in Transportation, Chicago, IL, August 2006, in review